

Is GW190521 the merger of black holes from the first stellar generations?

Eoin Farrell¹★, Jose H. Groh¹, Raphael Hirschi^{2,4}, Laura Murphy¹,
Etienne Kaiser², Sylvia Ekström³, Cyril Georgy³, Georges Meynet³

¹*School of Physics, Trinity College Dublin, The University of Dublin, Dublin, Ireland*

²*Astrophysics Group, Keele University, Keele, Staffordshire ST5 5BG, UK*

³*Geneva Observatory, University of Geneva, Chemin des Maillettes 51, 1290 Sauverny, Switzerland*

⁴*Institute for the Physics and Mathematic of the Universe (WPI), University of Tokyo, 5-1-5 Kashiwanoha, Kashiwa 277-8583, Japan*

Accepted XXX. Received YYY; in original form ZZZ

ABSTRACT

GW190521 challenges our understanding of the late-stage evolution of massive stars and the effects of the pair-instability in particular. We discuss the possibility that stars at low or zero metallicity could retain most of their hydrogen envelope until the pre-supernova stage, avoid the pulsational pair-instability regime and produce a black hole with a mass in the mass gap by fallback. We present a series of new stellar evolution models at zero and low metallicity computed with the Geneva and MESA stellar evolution codes and compare to existing grids of models. Models with a metallicity in the range $0 - 0.0004$ have three properties which favour higher BH masses. These are (i) lower mass-loss rates during the post-MS phase, (ii) a more compact star disfavoured binary interaction and (iii) possible H-He shell interactions which lower the CO core mass. We conclude that it is possible that GW190521 may be the merger of black holes produced directly by massive stars from the first stellar generations. Our models indicate BH masses up to 70-75 M_{\odot} . Uncertainties related to convective mixing, mass loss, H-He shell interactions and pair-instability pulsations may increase this limit to $\sim 85M_{\odot}$.

Key words: stars: evolution – stars: massive – stars: mass loss – stars: black holes

1 INTRODUCTION

The binary black hole merger GW190521 reported by the LIGO VIRGO Collaboration (The LIGO Scientific Collaboration et al. 2020a,b) contains unusually high component masses of 85^{+21}_{-14} and $66^{+17}_{-18} M_{\odot}$. These black hole masses lie within the mass gap predicted by standard (pulsational) pair-instability supernova theory. In this Letter we investigate the possibility that stars at low or zero metallicity could retain most of their hydrogen envelope until the pre-supernova stage, avoid the pulsational pair-instability regime and produce a black hole with a mass in the pair-instability mass gap.

In stars with CO core masses, $M_{\text{CO}} \gtrsim 30M_{\odot}$, the late nuclear burning phases are expected to be interrupted by the production of electron-positron pairs in the core (Fowler & Hoyle 1964; Rakavy et al. 1967). For stars with CO core masses of $30M_{\odot} \lesssim M_{\text{CO}} \lesssim 60M_{\odot}$, this can result in a series of energetic pulses followed by a collapse to a BH called a pulsational pair instability supernovae (PPISN) (Chatzopoulos & Wheeler 2012; Chen et al. 2014; Woosley 2017; Marchant et al. 2019; Leung et al. 2019). For $60M_{\odot} \lesssim M_{\text{CO}} \lesssim 120M_{\odot}$, pair creation can result in a complete disruption of the star in a pair-instability supernova (PISN), leaving behind no remnant

(Glatzel et al. 1985; Fryer et al. 2001; Umeda & Nomoto 2002; Kasen et al. 2011). For even higher M_{CO} , energy losses due to photo-disintegration are expected to result in a direct collapse to a BH (Fowler & Hoyle 1964; Ober et al. 1983; Heger et al. 2003; Woosley et al. 2007). The combined effect of PPI and PI is predicted to produce a gap in the BH birth mass distribution between $\sim 55 - 130M_{\odot}$ (Heger et al. 2003; Belczynski et al. 2016; Woosley 2019; Giacobbo et al. 2018). The exact boundaries of the mass gap are uncertain due to uncertainties in stellar evolution, core-collapse supernovae, PPISNe and PISNe (Woosley 2017; Mapelli et al. 2020; Marchant et al. 2019; Farmer et al. 2019; Stevenson et al. 2019; Renzo et al. 2020). Farmer et al. (2019) found that the lower boundary of the mass gap is quite robust against uncertainties in the metallicity ($\sim 3M_{\odot}$), internal mixing ($\sim 1M_{\odot}$) and stellar wind mass loss ($\sim 4M_{\odot}$). However, they found that varying the $^{12}\text{C}(\alpha, \gamma)^{16}\text{O}$ reaction rate within 1σ uncertainties shifts the location of the lower-boundary of the mass gap between 40 and 56 M_{\odot} . van Son et al. (2020) investigated the possibility of super-Eddington accretion forming BHs in the mass gap, however they found no BBH with a combined mass $> 100M_{\odot}$. Additionally, Marchant & Moriya (2020) investigated the impact of stellar rotation on the location of the mass gap and found that the lower boundary may be shifted upwards by 4 - 15% depending on the efficiency of angular momentum transport. The boundaries of the

★ E-mail: efarrel4@tcd.ie

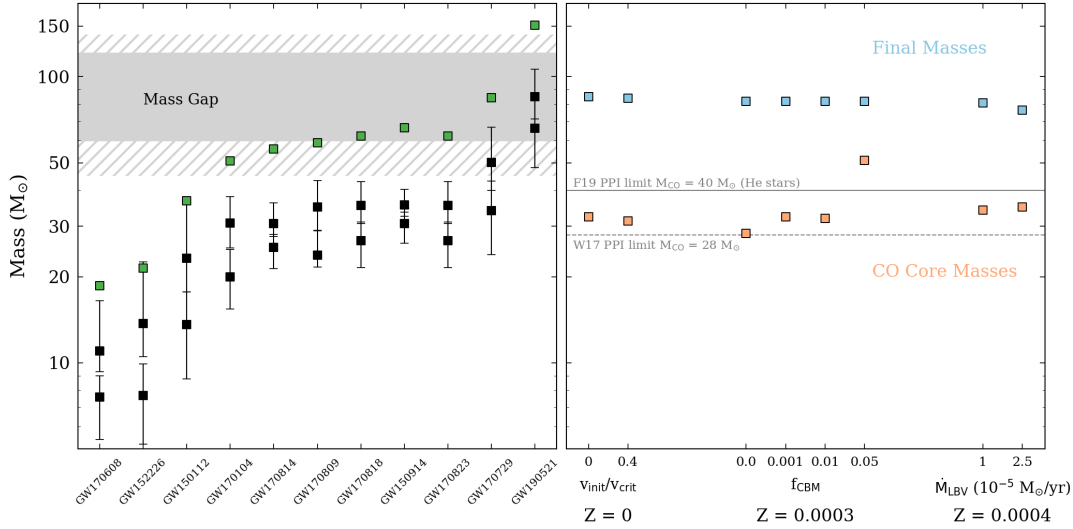


Figure 1. *Left panel:* Pre-merger and final BH masses from LIGO/Virgo observations in O1/O2 with GW190521 and the predicted region of the mass gap due to pair-instability. *Right panel:* Final masses (blue) and CO core masses (red) of selected $85M_{\odot}$ models listed in Table 1. We also include the maximum CO core mass found by Woosley (2017) that avoids any pulsations due to pair-instability.

pair-instability mass gap have also been proposed as a mechanism to place constraints on nuclear reaction rates (Farmer et al. 2020), particle physics (Croon et al. 2020) and in cosmological studies (Farr et al. 2019).

Based on the BH mass function predicted by PPISNe and PISNe, the observation of a pre-merger $\sim 85M_{\odot}$ BH as in GW190521 is unexpected. Several possibilities to create black holes with the reported mass are presented in previous works. The BH could form as a result of hierarchical mergers in dense stellar clusters, i.e. it is the result of the prior merger of two or more other BHs (e.g. Miller & Hamilton 2002; Gerosa & Berti 2017; Fishbach et al. 2017; Rodriguez et al. 2019; Romero-Shaw et al. 2020; Gayathri et al. 2020; Fragione et al. 2020). Other possible explanations include a stellar merger between a post-main sequence star and a main sequence binary companion (Spera et al. 2019; Di Carlo et al. 2019), a primordial origin De Luca et al. (2020), different assumptions for stellar wind mass loss Belczynski et al. (2020), Population III stars in binary systems (Kinugawa et al. 2020a,b; Tanikawa et al. 2020), an alternative prior in the gravitational wave analysis (Fishbach & Holz 2020) and modifications to the Standard Model of particle physics (Sakstein et al. 2020). The LIGO Scientific Collaboration et al. (2020b) found alternative explanations for the source of GW190521 to be highly unlikely, including a strongly gravitationally lensed merger or a highly eccentric merger. Given the widely predicted existence of the mass gap and the apparent robustness of the boundary of the gap with respect to uncertainties in stellar evolution models, can a single star produce a BH remnant with a mass around $85M_{\odot}$?

2 STELLAR EVOLUTION MODELS

We present a series of new stellar evolution models computed with the Geneva Stellar Evolution code, GENEC (Ekström et al. 2012; Murphy et al. in prep) and with MESA (r10398, Paxton et al. 2011, 2013, 2015). We also discuss the results from existing GENEC model grids (Ekström et al. 2012; Georgy et al. 2013; Groh et al. 2019). Except where otherwise stated, the input physics for the GENEC and MESA models are similar to those described in Ekström et al. (2012) and Choi et al. (2016), respectively. In our MESA models, we use the

Ledoux criterion for convection with an exponential overshooting parameterised by f_{CBM} , while in our GENEC models, we use the Schwarzschild criterion with step-overshooting parameterised by α_{ov} . In most models, we compute the evolution until at least the end of central C burning. For some GENEC rotating models, the computation is stopped at the end of He burning due to convergence difficulties. We define the CO core mass as the region where the helium abundance $Y < 0.01$ at the end of the evolution. The outputs from our models are summarised in Table 1.

Figure 1 compares the LIGO binary black hole (BBH) masses (Abbott et al. 2019) with the final masses and CO core masses of our models. The $85M_{\odot}$ models with Z in the range 0 to 0.0004 have final masses ranging from 76 to $85M_{\odot}$ and CO core masses ranging from 28 to $51M_{\odot}$. In this metallicity range, the final mass depends on assumptions about convective boundary mixing and post-MS mass loss. Not surprisingly, the model with the lowest amount of convective boundary mixing ($f_{\text{CBM}} = 0$ and with the Ledoux criterion) produces the lowest CO core mass of $28M_{\odot}$. Increasing convective boundary mixing tends to produce higher CO core masses, however this depends on whether H-He shell interactions modify the convective core mass during Helium burning. For instance, H-He shell interactions impact the model with $f_{\text{CBM}} = 0.01$ at $Z = 0.0003$ so that despite the larger overshooting, its final CO core mass is lower than the model with $f_{\text{CBM}} = 0.001$.

H-He shell interactions are an interesting possibility to reduce the final CO core masses of massive stars at low and zero Z (Ekström et al. 2008; Clarkson & Herwig 2020). This is relevant as it may allow a star to avoid the pulsational-pair instability regime, depending on initial mass and metallicity. To demonstrate this, we plot the Kippenhahn diagram of the evolution of our non-rotating $85M_{\odot}$ $Z = 0$ stellar model (Fig. 2). As expected, the convective core mass decreases during the MS evolution and increases following the onset of He-burning. However, shortly after the beginning of He-burning, the H-shell burning region becomes convective. This causes the convective core mass to decrease by $\sim 5M_{\odot}$ (inset plot in Fig. 2) and prevents any subsequent increase as the star evolves to the end of He-burning.

Figure 3 shows the evolutionary tracks in the Hertzsprung-

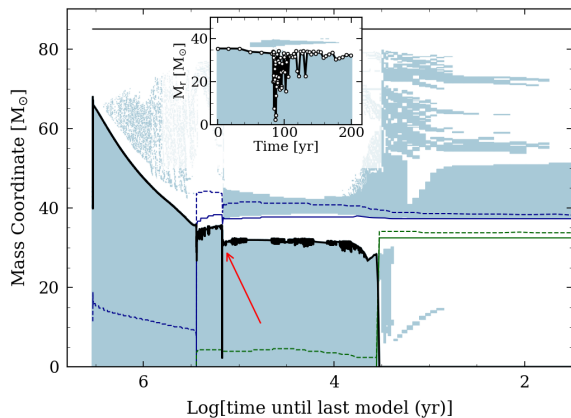


Figure 2. Kippenhahn diagram of a GENEC non-rotating $85 M_{\odot}$ model at $Z = 0$. Solid (dashed) lines correspond to the peak (100 erg/g/s) of the energy generation rate for H burning (blue) and He burning (green). The red arrow indicates the H-He shell interaction. An inset is included at the top of the figure to show that the interaction is resolved, where white circles indicate each timestep.

Russell diagram of three $85 M_{\odot}$ models with metallicities of $Z = 0$, 10^{-6} and 0.0003 . The qualitative evolution during the MS is similar for all models. The location of the zero-age main sequence moves to higher T_{eff} and luminosity with decreasing metallicity due the lower CNO abundances in the core. The post-MS evolution is affected in a similar way by the metallicity. At lower metallicities, a lower CNO abundance in the hydrogen-burning shell favours a more compact envelope and a higher T_{eff} . This trend continues until the pre-supernova stage, so that the maximum radii that the models reach are 142 , 672 and $794 R_{\odot}$ for $Z = 0$, 10^{-6} and 0.0003 respectively.

Previous works have focused on the context of producing BHs in close binary systems that could easily merge in the Hubble time and as a result assume that the entire H envelope will be lost to some combination of stellar winds, LBV eruptions or binary interaction (e.g. Farmer et al. 2019). As a result, they focus on the evolution and deaths of helium stars (e.g. Woosley 2019). For single stars with hydrogen envelopes, a maximum BH mass of 60 - $65 M_{\odot}$ has been suggested for non-rotating models (Woosley 2017; Mapelli et al. 2020; Spera & Mapelli 2017). In their models, strong mass loss of the higher mass models coupled with higher core masses prevented the formation of higher mass BHs. Rotating models were found to have lower maximum BH masses. The models presented in this paper indicate black hole masses of up to 70 - $75 M_{\odot}$, and possibly up to $85 M_{\odot}$ depending on uncertainties related to convective mixing, mass loss, H-He shell interactions and pair-instability pulsations. Our models leave open the possibility of a mass gap above $85 M_{\odot}$. To properly infer the actual limits of the pair instability mass gap based on these models, we would need to compute a large grid of models with different initial masses, rotation rates and metallicities. We defer this to future work.

3 IMPLICATIONS FOR BLACK HOLE MASSES FROM THE FIRST STELLAR GENERATIONS

Our models with $Z = 0$ to 0.0004 have three properties which favour higher BH masses as compared to higher metallicity models. These are (i) lower mass-loss rates, in particular during the post-MS phase, (ii) possible H-He shell interactions which lower the CO core mass and (iii) a more compact star disfavours binary interaction.

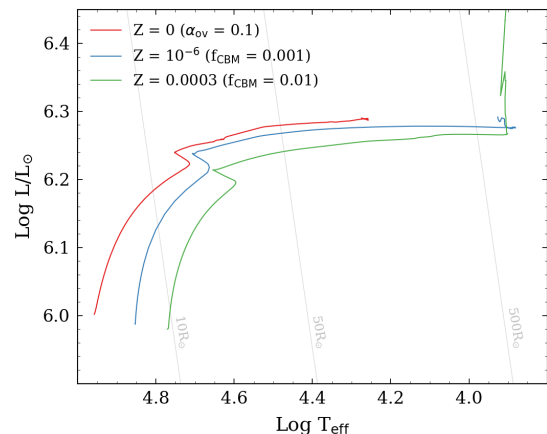


Figure 3. Evolutionary tracks of selected $85 M_{\odot}$ models in the Hertzsprung-Russell diagram with $Z = 0$, $Z = 10^{-6}$ and $Z = 0.0003$.

Table 1. Summary of our stellar evolution models. CBM refers to the free parameter regulating convective boundary mixing.

Z	M_{Zams} M_{\odot}	CBM $\alpha_{\text{ov}}/f_{\text{CBM}}$	Mass lost M_{\odot}	$M_{\text{final}}^{\text{tot}}$ M_{\odot}	$M_{\text{final}}^{\text{CO}}$ M_{\odot}	R_{max} R_{\odot}
Standard GENEC non-rotating models (α_{ov} value given for CBM)						
0	60	0.1	0.0	60.0	24.0	35
0	85	0.1	0.0	85.0	32.4	142
0	120	0.1	0.0	120.0	54.4	219
Standard GENEC rotating models ($v = 0.4 v_{\text{crit}}$)						
0	60	0.1	0.3	59.7	20.9	56
0	85	0.1	1.0	84.0	31.3	90
0	120	0.1	3.5	116.5	56.4	107
MESA models (f_{CBM} value given for CBM)						
10^{-6}	85	0.001	0.30	84.7	34.4	794
0.0003	85	0.0	3.0	82	28.3	766
0.0003	85	0.001	3.2	81.7	32.3	1169
0.0003	85	0.01	3.0	82	32.0	672
0.0003	85	0.05	7.0	78	51.0	984

3.1 Lower Mass Loss During the Evolution

The amount of mass that a star retains until the pre-supernova stage depends strongly on its metallicity (e.g., Groh et al. 2019). This is a result of the strong dependence of mass loss from radiative-driven winds on metallicity (Vink et al. 2001). For solar metallicity stars, the time-averaged mass-loss rate during the LBV phase and the presence of surface magnetic fields are important factors that determine the final BH mass of massive stars, which can range from 35 to $71 M_{\odot}$ for an $85 M_{\odot}$ star (Groh et al. 2020). At low metallicity, mass loss by stellar winds during the main-sequence phase becomes very low. Our $85 M_{\odot}$ models at $Z = 0.0003$ lose only $1.5 M_{\odot}$ during the MS assuming the Vink et al. (2001) prescription. Further mass loss occurs during the post-MS and is strongly dependent on how cool the surface becomes. Our $Z = 0.0003$ MESA models stay hot and lose $1.5 M_{\odot}$ during the post-MS, while our GENEC models can become spectroscopically similar to LBVs (Groh et al. 2014). As a result, they may lose significantly more mass at that stage ($7.5 M_{\odot}$ for $\dot{M}_{\text{LBV,max}} = 2.5 \times 10^{-5} M_{\odot}/\text{yr}$), even at low metallicity (Smith & Owocki 2006; Allan et al. 2020).

At zero metallicity, radiatively driven mass loss becomes negligible throughout the evolution (Krtićka & Kubát 2006), although for fast rotating stars there can be some small mass loss if the critical rotation limit is reached. Zero or negligible mass loss has been customarily used in stellar evolution grids at zero metallicity such as Marigo et al. (2001); Ekström et al. (2008); Yoon et al. (2012); Windhorst et al. (2018) and Murphy et al. 2020, in prep. As such, our zero-metallicity models retain most of their mass until core collapse. There is little observational constraints for mass-loss rates at these extremely low- Z values, in particular for the post-MS stages, and we should regard our assumptions about mass-loss rates as highly uncertain. Uncertainties related to mass-loss rates may affect both the final mass, the CO core mass and the maximum radius.

3.2 Possibility of H-He Shell Interactions

Some of our models at low/zero metallicity experience strong H-He shell interactions (Fig. 2). This behaviour has been seen in previous low metallicity stellar evolution models (e.g. Chieffi & Limongi 2004; Ekström et al. 2008; Ritter et al. 2018; Clarkson & Herwig 2020). During He-burning, a low or zero abundance of CNO elements in the H-burning shell favours a bluer star which increases the likelihood of the H-burning region becoming convective and subsequently reducing the convective core mass. In models with $Z = 0$, diffusion of C from the He-burning core to the H-burning shell can trigger a strong CNO cycle boost, make the shell convective and lead to H-He shell interactions. By comparing the GENEC models for metallicities of $Z = 0.0004, 0.002$ and 0.014 , Groh et al. (2019) discuss that the occurrence of H-He shell interactions may be favoured at lower metallicities. Clarkson & Herwig (2020) find different types of H-He shell interactions that occur at different times during the evolution. Some of these interactions, particularly during the late stages, may dramatically reduce the CO core mass and allow the star to avoid the pulsational pair instability regime. We encourage further work on the effects of convective boundary mixing and rotation on H-He shell interactions as this is crucial for understanding the fate of massive stars at low and zero metallicity.

Some of our models assume a relatively low amount of convective overshooting. The extent and implementation of convective overshooting in stellar models has a large impact on the mass of the He and CO cores (e.g. Kaiser et al. 2020). Three-dimensional models of lower mass stars favour the existence of such mixing at convective boundaries (e.g. Cristini et al. 2017), although it is still unclear how it is affected by other parameters such as mass and metallicity. In addition, for stars of initial mass $7 < M_{\text{init}} < 25M_{\odot}$ a high value of f_{CBM} is favoured (Martinet et al. 2020, in prep) as well as for masses of $\sim 35M_{\odot}$ (Higgins & Vink 2019). However, these constraints are for core-H burning stars. The value of f_{CBM} is not as well constrained for other burning phases or for stars of $\sim 85M_{\odot}$ which have different internal structures to $\sim 15M_{\odot}$ stars and larger core mass ratios.

3.3 Smaller Radius disfavours Binary Interaction

Zero-metallicity models favour the retention of the H-envelope in binary systems because they are more compact than higher metallicity stars. For example, the maximum radius of our $85M_{\odot}$ rotating model at $Z = 0$ is $R_{\text{max}} = 142R_{\odot}$, as compared to $952R_{\odot}$ at $Z = 0.0004$ and $815R_{\odot}$ at $Z = 0.014$. The radius of stellar models at these masses depends greatly on the assumptions for convection in the envelope (e.g. Gräfenener et al. 2012; Jiang et al. 2018). Additionally, the radius is

strongly impacted by uncertainties related to the chemical abundance profile in the envelope (Farrell et al. 2020), which is impacted by the properties of mixing (e.g. Schootemeijer et al. 2019). The size and interaction of convective shells above the core during the MS and between the MS and He-burning greatly affect the radius of the star during He-burning. If these processes result in hydrogen being mixed into the H-shell burning region, the star will remain more compact for longer during He-burning.

Binary interactions may also provide a mechanism to produce a pre-supernova structure with a high hydrogen envelope mass (e.g. Justham et al. 2014). Mass gainers or products of mergers during the post-MS that do not fully rejuvenate could have low core masses and large envelope masses, potentially avoiding the PPI regime and collapsing to a black hole with the H envelope falling back onto the BH (Spera et al. 2019; Di Carlo et al. 2019).

3.4 Pulsational Pair-Instability

Models suggest that stars with a CO core mass of $\geq 28M_{\odot}$ will undergo pair-instability driven pulsation during their final stages (Woosley 2017). For example, Woosley (2017) present a model (T80D) with a final mass of $80M_{\odot}$ and a CO core mass of $32.6M_{\odot}$ that, due to pulsations, will produce a final BH mass of $34.9M_{\odot}$. The exact value of the maximum CO core mass of this boundary that will avoid the pair-instability is uncertain (e.g. Woosley 2017; Farmer et al. 2019; Marchant et al. 2019) and effects related to convective boundary mixing, stellar winds and the $^{12}\text{C}(\alpha, \gamma)^{16}\text{O}$ reaction rate may increase this value. Our $60M_{\odot}$ models with $Z = 0$ have CO core masses between 21 and $24M_{\odot}$. Most of our $85M_{\odot}$ models are just above this strict limit with CO core masses of $31 - 35M_{\odot}$. We computed a test model with no convective boundary mixing that finishes with a CO core mass of $28M_{\odot}$. By interpolating between our 60 and $85M_{\odot}$ models, we compute that a $72M_{\odot}$ model will have a final CO core mass of $28M_{\odot}$ under the standard assumptions for convection in the GENEC models.

For a pulse of a given energy, the amount of mass that a star loses depends on the binding energy of the envelope. More compact, hotter stars are less likely to lose their entire H envelope compared to extended envelopes, such as in RSGs. For this reason, $Z = 0$ models are favoured to retain large masses as they remain compact until the end of their evolution. Farmer et al. (2019) find a CO core mass limit for the onset of PPI of $\sim 40M_{\odot}$ for highly compact helium stars. Since our models are hydrogen rich, with a lower binding energy than helium stars, it is unclear if this limit would apply to our $85M_{\odot}$ models. Further studies could investigate the impact of the uncertainties discussed by Farmer et al. (2019), such as the $^{12}\text{C}(\alpha, \gamma)^{16}\text{O}$ reaction rate, in hydrogen-rich models that are blue and relatively compact, such as our $Z = 0$ models. If the pulses are not present and/or do not remove the H envelope, this may allow the formation of $85M_{\odot}$ BHs.

4 IMPACTS FOR BINARY BLACK HOLE MERGERS

Due to their lower mass-loss rates, smaller radii and the possibility of H-He shell interactions that reduce the CO core mass, stars in the first stellar generations are ideal candidates to produce BHs in the mass gap such as GW190521, with masses of $70 - 75M_{\odot}$. In order to produce a BBH merger observable by LIGO/Virgo, such a BH would need to be in a close binary system. Due to uncertainties in the evolution of massive stars and in how these stars behave in binary systems, it is difficult to perfectly constrain the possible evolutionary pathways that would lead to a system. Despite their large H-envelope

mass, our models at $Z = 0$ expand only to radii $\sim 100R_{\odot}$. If the star has a binary companion and avoids Roche-Lobe overflow, the merging timescale would likely exceed the Hubble time. However, if the orbital separation were to reduce after the more massive star dies (e.g. due to a common envelope phase) this may reduce the merging timescale. Alternatively, if the BH is in a dense stellar cluster, it could dynamically capture a companion and form a close binary system (e.g. Sigurdsson & Hernquist 1993; Portegies Zwart & McMillan 2000; Downing et al. 2010; Rodriguez et al. 2016). We leave the details of the binary evolution scenario or dynamical capture to future work (e.g. Belczynski 2020).

Acknowledgements: EF, JHG and LM thank the Irish Research Council for funding. JHG thanks Isidoros and Giorgos for providing useful resources. This article is based upon work from the “ChETEC” COST Action (CA16117). RH acknowledges support from the IReNA AccelNet Network of Networks (NSF Grant No. OISE-1927130) and from the World Premier International Research Centre Initiative. CG has received funding from the ERC (grant No 833925).

Data availability: The derived data generated in this research will be shared on reasonable request to the corresponding author.

REFERENCES

- Abbott B. P., et al., 2019, *Physical Review X*, **9**, 031040
- Allan A. P., Groh J. H., Mehner A., Smith N., Boian I., Farrell E. J., Andrews J. E., 2020, *MNRAS*, **496**, 1902
- Belczynski K., 2020, arXiv e-prints, p. arXiv:2009.13526
- Belczynski K., et al., 2016, *A&A*, **594**, A97
- Belczynski K., et al., 2020, *ApJ*, **890**, 113
- Chatzopoulos E., Wheeler J. C., 2012, *ApJ*, **748**, 42
- Chen K.-J., Woosley S., Heger A., Almgren A., Whalen D. J., 2014, *ApJ*, **792**, 28
- Chieffi A., Limongi M., 2004, *ApJ*, **608**, 405
- Choi J., Dotter A., Conroy C., Cantiello M., Paxton B., Johnson B. D., 2016, *ApJ*, **823**, 102
- Clarkson O., Herwig F., 2020, arXiv e-prints, p. arXiv:2005.07748
- Cristini A., Meakin C., Hirschi R., Arnett D., Georgy C., Viallet M., Walkington I., 2017, *MNRAS*, **471**, 279
- Croon D., McDermott S. D., Sakstein J., 2020, arXiv e-prints, p. arXiv:2007.07889
- De Luca V., Desjacques V., Franciolini G., Pani P., Riotto A., 2020, arXiv e-prints, p. arXiv:2009.01728
- Di Carlo U. N., Giacobbo N., Mapelli M., Pasquato M., Spera M., Wang L., Haardt F., 2019, *MNRAS*, **487**, 2947
- Downing J. M. B., Benacquista M. J., Giersz M., Spurzem R., 2010, *MNRAS*, **407**, 1946
- Ekström S., Meynet G., Chiappini C., Hirschi R., Maeder A., 2008, *A&A*, **489**, 685
- Ekström S., et al., 2012, *A&A*, **537**, A146
- Farmer R., Renzo M., de Mink S. E., Marchant P., Justham S., 2019, *ApJ*, **887**, 53
- Farmer R., Renzo M., de Mink S., Fishbach M., Justham S., 2020, arXiv e-prints, p. arXiv:2006.06678
- Farr W. M., Fishbach M., Ye J., Holz D. E., 2019, *ApJ*, **883**, L42
- Farrell E. J., Groh J. H., Meynet G., Eldridge J. J., Ekström S., Georgy C., 2020, *MNRAS*, **495**, 4659
- Fishbach M., Holz D., 2020, arXiv e-prints, p. arXiv:2009.05472
- Fishbach M., Holz D. E., Farr B., 2017, *ApJ*, **840**, L24
- Fowler W. A., Hoyle F., 1964, *ApJS*, **9**, 201
- Fragione G., Loeb A., Rasio F., 2020, arXiv e-prints, p. arXiv:2009.05065
- Fryer C. L., Woosley S. E., Heger A., 2001, *ApJ*, **550**, 372
- Gayathri V., et al., 2020, arXiv e-prints, p. arXiv:2009.05461
- Georgy C., et al., 2013, *A&A*, **558**, A103
- Gerosa D., Berti E., 2017, *Phys. Rev. D*, **95**, 124046
- Giacobbo N., Mapelli M., Spera M., 2018, *MNRAS*, **474**, 2959
- Glatzel W., Fricke K. J., El Eid M. F., 1985, *A&A*, **149**, 413
- Gräfener G., Owocki S. P., Vink J. S., 2012, *A&A*, **538**, A40
- Groh J. H., Meynet G., Ekström S., Georgy C., 2014, *A&A*, **564**, A30
- Groh J. H., et al., 2019, *A&A*, **627**, A24
- Groh J. H., Farrell E. J., Meynet G., Smith N., Murphy L., Allan A. P., Georgy C., Ekstroem S., 2020, *ApJ*, **900**, 98
- Heger A., Fryer C. L., Woosley S. E., Langer N., Hartmann D. H., 2003, *ApJ*, **591**, 288
- Higgins E. R., Vink J. S., 2019, *A&A*, **622**, A50
- Jiang Y.-F., Cantiello M., Bildsten L., Quataert E., Blaes O., Stone J., 2018, *Nature*, **561**, 498
- Justham S., Podsiadlowski P., Vink J. S., 2014, *ApJ*, **796**, 121
- Kaiser E. A., Hirschi R., Arnett W. D., Georgy C., Scott L. J. A., Cristini A., 2020, *MNRAS*, **496**, 1967
- Kasen D., Woosley S. E., Heger A., 2011, *ApJ*, **734**, 102
- Kinugawa T., Nakamura T., Nakano H., 2020a, arXiv e-prints, p. arXiv:2009.06922
- Kinugawa T., Nakamura T., Nakano H., 2020b, *MNRAS*, **498**, 3946
- Krtićka J., Kubát J., 2006, *A&A*, **446**, 1039
- Leung S.-C., Nomoto K., Blinnikov S., 2019, *ApJ*, **887**, 72
- Mapelli M., Spera M., Montanari E., Limongi M., Chieffi A., Giacobbo N., Bressan A., Bouffanais Y., 2020, *ApJ*, **888**, 76
- Marchant P., Moriya T. J., 2020, *A&A*, **640**, L18
- Marchant P., Renzo M., Farmer R., Pappas K. M. W., Taam R. E., de Mink S. E., Kalogera V., 2019, *ApJ*, **882**, 36
- Marigo P., Girardi L., Chiosi C., Wood P. R., 2001, *A&A*, **371**, 152
- Miller M. C., Hamilton D. P., 2002, *MNRAS*, **330**, 232
- Ober W. W., El Eid M. F., Fricke K. J., 1983, *A&A*, **119**, 61
- Paxton B., Bildsten L., Dotter A., Herwig F., Lesaffre P., Timmes F., 2011, *ApJS*, **192**, 3
- Paxton B., et al., 2013, *ApJS*, **208**, 4
- Paxton B., et al., 2015, *ApJS*, **220**, 15
- Portegies Zwart S. F., McMillan S. L. W., 2000, *ApJ*, **528**, L17
- Rakavy G., Shaviv G., Zinamon Z., 1967, *ApJ*, **150**, 131
- Renzo M., Farmer R. J., Justham S., de Mink S. E., Götzberg Y., Marchant P., 2020, *MNRAS*, **493**, 4333
- Ritter C., Herwig F., Jones S., Pignatari M., Fryer C., Hirschi R., 2018, *MNRAS*, **480**, 538
- Rodriguez C. L., Zevin M., Pankow C., Kalogera V., Rasio F. A., 2016, *ApJ*, **832**, L2
- Rodriguez C. L., Zevin M., Amaro-Seoane P., Chatterjee S., Kremer K., Rasio F. A., Ye C. S., 2019, *Phys. Rev. D*, **100**, 043027
- Romero-Shaw I. M., Lasky P. D., Thrane E., Calderon Bustillo J., 2020, arXiv e-prints, p. arXiv:2009.04771
- Sakstein J., Croon D., McDermott S. D., Straight M. C., Baxter E. J., 2020, arXiv e-prints, p. arXiv:2009.01213
- Schootemeijer A., Langer N., Grin N. J., Wang C., 2019, *A&A*, **625**, A132
- Sigurdsson S., Hernquist L., 1993, *Nature*, **364**, 423
- Smith N., Owocki S. P., 2006, *ApJ*, **645**, L45
- Spera M., Mapelli M., 2017, *MNRAS*, **470**, 4739
- Spera M., Mapelli M., Giacobbo N., Trani A. A., Bressan A., Costa G., 2019, *MNRAS*, **485**, 889
- Stevenson S., Sampson M., Powell J., Vigna-Gómez A., Neijssel C. J., Szécsi D., Mandel I., 2019, *ApJ*, **882**, 121
- Tanikawa A., Susa H., Yoshida T., Trani A. A., Kinugawa T., 2020, arXiv e-prints, p. arXiv:2008.01890
- The LIGO Scientific Collaboration et al., 2020a, arXiv e-prints, p. arXiv:2009.01075
- The LIGO Scientific Collaboration et al., 2020b, arXiv e-prints, p. arXiv:2009.01190
- Umeda H., Nomoto K., 2002, *ApJ*, **565**, 385
- Vink J. S., de Koter A., Lamers H. J. G. L. M., 2001, *A&A*, **369**, 574
- Windhorst R. A., et al., 2018, *ApJS*, **234**, 41
- Woosley S. E., 2017, *ApJ*, **836**, 244
- Woosley S. E., 2019, *ApJ*, **878**, 49
- Woosley S. E., Blinnikov S., Heger A., 2007, *Nature*, **450**, 390
- Yoon S. C., Dierks A., Langer N., 2012, *A&A*, **542**, A113
- van Son L. A. C., et al., 2020, *ApJ*, **897**, 100